Functionality of potato virus Y coat protein in cell-to-cell movement dynamics is defined by its N terminal region

Anže Vozelj[1,2*], Tjaša Mahkovec Povalej[1], Katja Stare[1], Magda Tušek Žnidarič[1], Katarina Bačnik[1], Valentina Levak[1,2], Ion Gutiérrez-Aguirre[1], Marjetka Podobnik[3], Kristina Gruden[1], Anna Coll[1]†, Tjaša Lukan[1]†*

[1]Department of Biotechnology and Systems Biology, National Institute of Biology, Večna pot 121, 1000 Ljubljana, Slovenia

[2]Jožef Stefan International Postgraduate School, Jamova cesta 39, 1000 Ljubljana, Slovenia

[3]Department of Molecular Biology and Nanobiotechnology, National Institute of Chemistry, Hajdrihova 19, 1001 Ljubljana, Slovenia

* Corresponding authors.

Email: anze.vozelj@nib.si, tjasa.lukan@nib.si

† shared last authorship

Abstract

Potato virus Y (PVY) is one of the top ten economically most important plant viruses and responsible for major yield losses. We previously suggested the involvement of the N terminal region of potato virus Y coat protein (CP) in PVY spread. By constructing different N terminal deletion mutants of PVY N605 strain, we here show that deletions of 40 or more amino acid residues from the N terminal region of the CP resulted in the PVY multiplication limited to primary infected cells in *Nicotiana clevelandii* plants. Deletion of 26 residues profoundly impaired PVY cell-to-cell movement and prevented systemic PVY spread, while deletions of 19-23 residues allowed delayed systemic PVY spread. Introduced point mutations in the identified region prevent (S21G) or delay (G20P) PVY movement. In summary, this work shows the significance of the CP N-terminus for movement of the PVY.

Keywords: potato virus Y, potato (*Solanum tuberosum*), coat protein (CP), viral movement, point mutations

Introduction

Plants undergo constant exposure to various pathogens and pests, with viruses being the most severe amongst them. Potato virus Y (PVY) is classified amongst the top ten economically most important plant viruses infecting solanaceous crops including potato, tomato, tobacco and pepper (1). PVY is the causal agent of potato tuber necrosis ringspot disease (2), a devastating disease that negatively impacts potato tuber quality and yield (3).

PVY belongs to the *Potyvirus* genus. Its genome consists of 9,7-kb positive sense single stranded RNA (+ ssRNA) encoding for single open reading frame (ORF) that is translated into 350 kDa long polyprotein which is cleaved into 10 mature proteins (3). Furthermore, PVY genome contains an additional ORF *pipo* ("pretty interesting *potyviridae* ORF"), embedded within the P3 cistron of the polyprotein. Expression of *pipo* occurs through transcriptional slippage by the viral RNA polymerase and results in production of the P3N-PIPO fusion protein, which is involved in cell to cell movement (4, 5).

The majority of potyviral proteins are multifunctional and they altogether contribute to the establishment of successful viral infection, that encompasses multiple steps including transmission by aphids, penetration of viral particles into the cell, virion disassembly, translation, replication, suppression of host defense mechanisms, virion assembly and virus movement from the primary infected cells to neighboring cells and systemic spread (6).

Viral movement is facilitated through plasmodesmata, plant specific structures connecting two adjacent cells that serve as gateways for cell-to-cell movement and contribute to the establishment of systemic infection (7, 8, 9, 10). At least four potyviral proteins, coat protein (CP), cylindrical inclusion protein (CI), P3N-PIPO and the second 6 kDa protein (6K2) protein are essential for cell-to-cell movement of potyviruses (11). P3N-PIPO is localized in the plasmodesmata and directs CI to form conical structures that are crucial for assistance of potyviral intercellular movement through plasmodesmata, which was shown for turnip mosaic virus (TuMV) in *Nicotiana benthamiana* (12). Accumulation of CP in plasmodesmata during infection is also crucial since together with the

62 potyviral Helper-Component Proteinase (HCPro) increases the size exclusion limit (SEL) of
63 plasmodesmata, which was determined by microinjection studies for bean common mosaic
64 necrosis potyvirus (BCMNV) in *N. benthamiana* (13). Systemic infection encompasses viral
65 movement through phloem and less often through xylem to reach and infect plant distant tissues
66 (14, 15). However, before reaching vasculature, plant viruses need to cross various cellular barriers
67 including bundle sheath, vascular parenchyma and companion cells, to reach sieve elements,
68 through which they are transported to distant tissues (14). The invasion of distant tissues requires
69 unloading from sieve elements into companion cells and cell-to-cell movement into bundle sheath
70 and mesophyll cells (14). Despite PVY being one of the most extensively studied potyviruses on
71 molecular scale, information about crucial factors governing cell-to-cell as well as systemic spread
72 are scarce (6, 11).

73 The cryo-EM structures of some potyviruses including PVY, watermelon mosaic virus (WMV) and
74 TuMV virions have been determined and offered a detailed insight into the conserved helical
75 arrangement of CPs assembled around viral ssRNA as well as the conserved three dimensional
76 structure of CP among them (17, 16, 18). CP is the only potyviral structural protein and more than
77 2000 copies of CP encapsidate the viral ssRNA molecule to form potyviral virions (6, 10). Individual
78 CP is built of three distinct regions. The N terminal region with residues up to Val44 in PVY, which
79 are exposed at the outer surface of the virus, are flexible and thus its 3D structure was not
80 determined. The rest of N terminal region, from Val44 to Gln76, is structured. It has an extended
81 structure with one short alpha helix in the middle (17). The central core has a globular shape. The
82 C terminal region is in the lumen of the virus and its extended structure is supported by the viral
83 ssRNA scaffold (17). Beyond its primary role in viral encapsidation, the CP is indispensable for
84 aphid transmission, potyviral RNA amplification and cell-to-cell movement (10, 13, 19). Functional
85 studies of the CP protein indicate crucial roles of its N and C terminal regions and the core region
86 in potyvirus infectivity. In the case of PVY, the absence of the flexible CP N terminal region hinders
87 the formation of filaments and cell-to-cell viral movement (17). For soybean mosaic virus (SMV),
88 the CP C terminal region is involved in CP intersubunit interactions, viral cell-to-cell and long

89 distance movement and virion assembly (20). In potato virus A (PVA), phosphorylation of Thr243
90 residue on CP C terminal region is crucial for PVA replication *in planta* (21). These results and
91 results of several other studies suggest that different CP regions are important for cell-to-cell
92 movement of potyviruses (22, 23, 24, 25, 26, 27). It is not known yet in what structural shape are
93 the viruses propagated through the plant, as assembled virions or viral ribonucleoprotein (RNP)
94 complexes associated with CP (14, 15).

95 The so far generated evidence-based knowledge differs from one potyvirus to another, and thus,
96 more research is needed to comprehensively elucidate these complex processes, particularly for
97 those economically relevant potyviruses such as PVY. By constructing different PVY N terminal
98 deletion mutants, we identified the regions of the CP that are important for efficient PVY cell-to-cell
99 movement.

100

101 **Results**
102
103 **Deletion of 40 or more amino acid residues from the PVY CP N terminal region affects cell-**
104 **to-cell movement, but does not prevent replication**

105 Previously we showed that PVY with deleted 50 N terminal amino acid residues was still able to
106 replicate but based on the low and spatially limited levels of RNA accumulation, we suggested that
107 N terminal region is required for cell-to-cell movement (17). To confirm this hypothesis, we here
108 constructed two GFP-tagged PVY (PVY N605-GFP) mutants lacking either 40 or 50 amino acid
109 residues at the CP N terminal region (hereafter ΔN50-CP and ΔN40-CP). In all constructed mutants
110 GFP was inserted between NIb and CP coding sequence, flanked by protease recognition sites,
111 allowing GFP excision from the polyprotein after translation (28). We followed the spread of ΔN50-
112 CP and ΔN40-CP with confocal microscopy upon bombardment of *Nicotiana clevelandii* leaves
113 (Fig. 1B). Neither mutant was able to move cell-to-cell, remaining limited to bombarded cells (Fig.
114 1B). We detected viral RNA replication of both mutants in the bombarded leaves, albeit at
115 significantly lower levels in comparison to the non-mutated clone (hereafter WT-CP) (Fig. S1, data
116 S1 and S2). Despite the lower RNA levels observed in leaves bombarded with constructed mutants,
117 confocal microscopy image analysis showed that the accumulation of GFP in individual infected
118 cells was the same in WT and ΔN40-CP mutant, confirming unhindered replication (Table S2).
119 These findings corroborate our previous results showing that N terminal region CP truncations still
120 allow viral replication (17) and further show that the absence of either 50 or 40 N-terminal residues
121 abolish cell-to-cell viral movement.

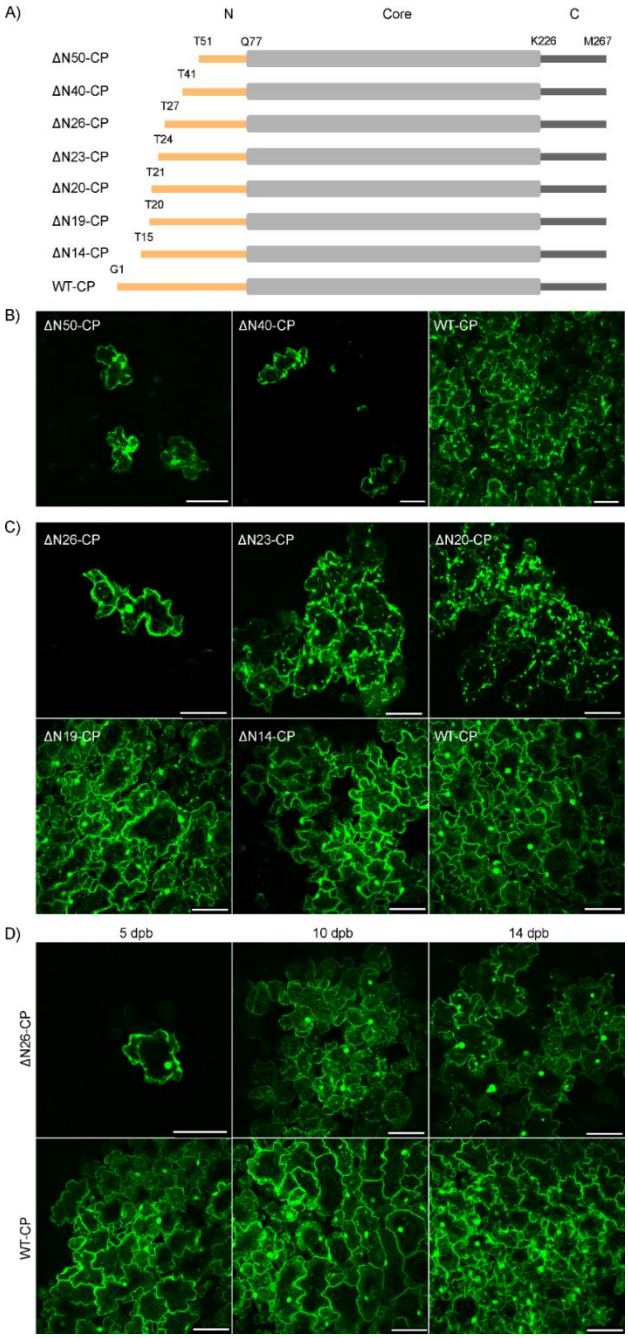

Figure 1. Amino acid deletions at PVY CP N terminal region influence viral cell-to-cell movement. **(A)** Schematic representation of constructed mutants with deletions on PVY CP N terminal region (N-terminal region, orange; core region, grey; C-terminal region, dark grey) with labeled amino acids. **(B)** Confocal microscopy images showing viral replication is limited to single cells when 50 (ΔN50-CP) or 40 (ΔN40-CP) amino acid residues were deleted at CP N terminal region, while non-mutated clone (WT-CP) shows cell-to-cell spread 10-12 days post bombardment (dpb). Scale bar: 100 μm. **(C)** 5 dpb viral replication is limited to

130 single cells in ΔN26-CP mutant, while cell-to-cell virus spread was observed for CP deletion mutants ΔN23-
131 CP, ΔN20-CP, ΔN19-CP, ΔN14-CP. Scale bar: 100 µm. **(D)** ΔN26-CP cell-to cell-spread was observed at later
132 time points (10 and 14 dpb). Scale bar: 100 µm.

133 **The deletions of 19-26 amino acid residues of the PVY CP N terminal region are influencing**
134 **dynamics of viral cell-to-cell spread**

135 To further assess which region of CP N terminal is crucial for cell-to-cell virus spread, we
136 constructed GFP-tagged mutants lacking 26, 23, 20, 19 and 14 amino acid residues at the CP N
137 terminal region (Fig. 1A) and followed their localization under confocal microscope at different time
138 points after virus inoculation (Fig. 1, C and D, data S2 and table S1). Mutants lacking 26 (ΔN26 -
139 CP) and 23 (ΔN23 -CP) residues on CP N terminal region had the first non deleted amino acid
140 replaced with glycine (G) during the mutagenesis.

141 At 5 dpb, ΔN14-CP and ΔN19-CP mutants did not show any differences in cell-to-cell spread
142 compared to WT-CP, while a lower spread level was noticed for ΔN20-CP and ΔN23-CP (Fig. 1C).
143 The most pronounced difference in comparison to other mutants and to WT-CP was observed in
144 the case of ΔN26-CP mutant, which remained confined to single cells at 5 dpb (Fig. 1, C and D).
145 However, at later timepoints (10 and 14 dpb), in approximately half of the infected plants, we also
146 observed cell-to-cell viral movement, although substantially delayed compared to WT-CP (Fig. 1D
147 and table S1). Also, the measured viral RNA load for ΔN26-CP mutant was significantly lower than
148 that of WT-CP at all 5 dpb, 10 and 14 dpb (Fig. S2 and data S1).

149 Whole plant imaging was conducted to more precisely examine the dynamics of cell-to-cell virus
150 spread of WT-CP, ΔN23-CP, ΔN19-CP and ΔN14-CP through time on inoculated *N. clevelandii*
151 leaves (Fig. 2A). As expected, the results revealed statistically significant differences in the viral
152 multiplication area between N23-CP and WT-CP, and ΔN19-CP compared to WT-CP (Fig. 2, B and
153 C and data S3 and S4). A similar though less evident trend was observed in the case of ΔN14-CP
154 compared to WT-CP, which was not statistically significant (Fig.2 C and data S4).

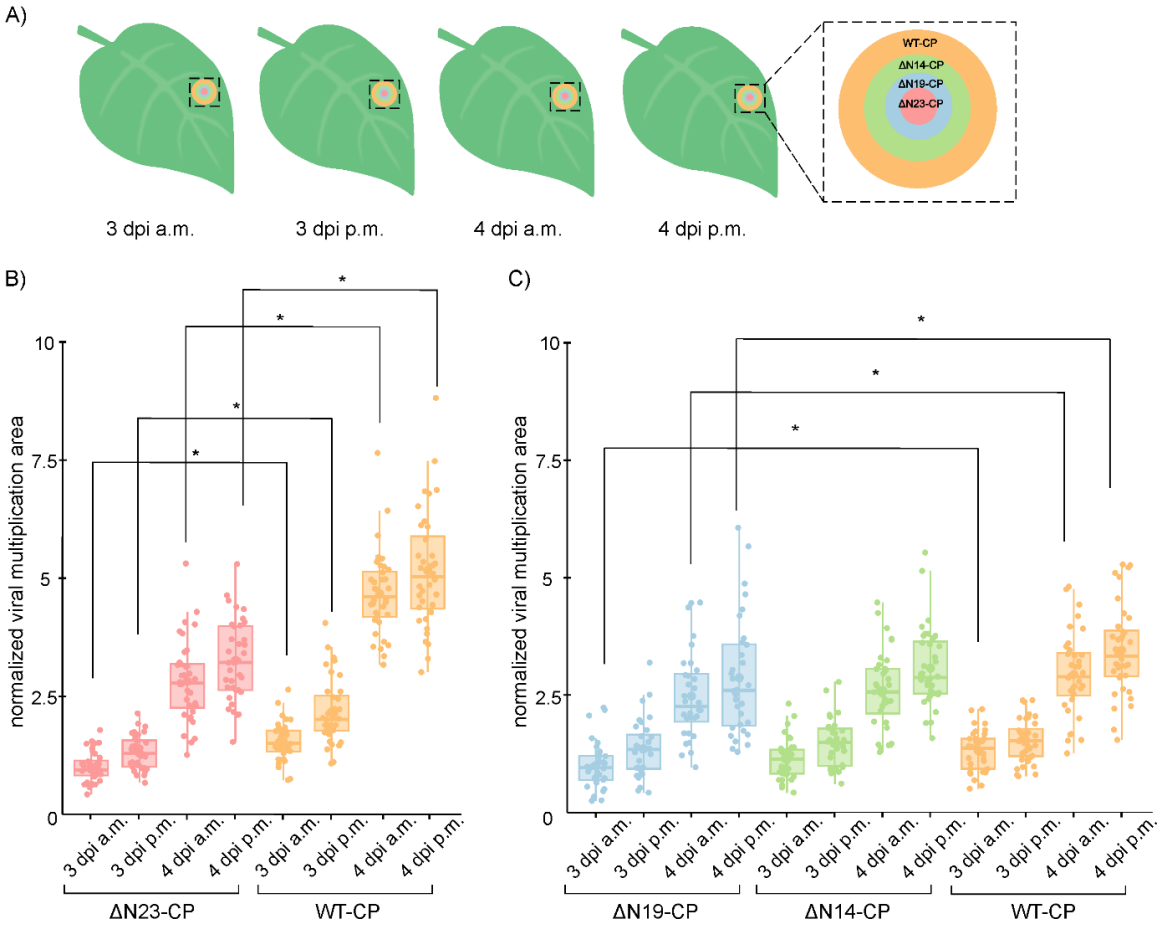

Figure 2. Precise analysis of the viral multiplication areas revealed a hampered cell-to-cell virus spread in ΔN19-CP and ΔN23-CP mutants. (A) The scheme of the viral multiplication area at different time points for all mutants compared with WT-CP. The area was followed by more precise analysis using whole plant imaging system for examining cell-to-cell virus spread of ΔN23-CP, ΔN19-CP, ΔN14-CP and WT-CP in four timepoints including 3 days post inoculation (dpi) in the morning (a.m), 3 dpi in the afternoon (p.m), 4 dpi a.m. and 4 dpi p.m. Note that the viral multiplication area was the largest after infection with WT-CP and decreased in the latter order ΔN14-CP, ΔN19-CP and ΔN23-CP. **(B and C)** Normalized viral multiplication area. After inoculating leaves with WT-CP or mutants, plants were imaged with whole plant imaging system. Images of three selected viral multiplication areas per leaf per plant were taken at four time points. Differences were statistically evaluated using Welch's t test. Results are presented as boxplots with dots representing normalized viral multiplication areas (data S3 and S4) for ΔN23-CP-CP, WT-CP **(B)** and ΔN19-CP, ΔN14-CP, WT-CP **(C)**. Statistically significant differences ($p < 0.05$) are denoted with an asterisk (*). Vertical lines present all points except outliers. Raw and normalized data, number of plants and statistics are specified in Data S3

169 and S4. The same trend was observed in a replicate experiment (Fig. S3 and data S5). For comparison
170 between two independent experiments, data measured for mutant viruses were normalized to median of
171 values obtained for WT virus (data S6).

172 These results show that the dynamics of viral cell-to-cell spread is dependent on the length of the
173 CP N terminal region (Fig. 1 and data S2). More precisely, as the number of CP N terminal region
174 deleted amino acid residues increases, cell-to-cell movement speed is decreased (Fig. 2, B and
175 C and data S3, S4 and S6). We conclude that amino acids in the region 19-26 on CP N terminal
176 region are essential for an optimal PVY cell-to-cell movement. Furthermore, with electron
177 microscopy we observed that viral assembly at all tested deletion mutants is feasible (Supp. Fig.
178 10).

179 **Systemic viral spread dynamics is affected by the cell-to-cell movement**

180 Since viral cell-to-cell spread is prerequisite for systemic viral spread, we further tested if the
181 observed delay in cell-to-cell viral spread of mutants (Figs. 1, C and 2, B and C) affects the systemic
182 viral spread. In contrast to the systemic spread of WT-CP, which is detectable already at 7 dpb, the
183 spread of ΔN23-CP, ΔN19-CP and ΔN14-CP mutants to systemic leaves occurs with a delay (Fig.
184 3A). If compared to WT-CP, ΔN14-CP was observed in systemic tissue with 1 day delay (8 dpb),
185 ΔN19-CP with 2 days delay (9 dpb) and ΔN23-CP with approximately 3 weeks delay (25 dpb) (Fig.
186 3A). The mutant ΔN26-CP did not reach systemic leaves even at the highest tested dpb (Fig. S4).

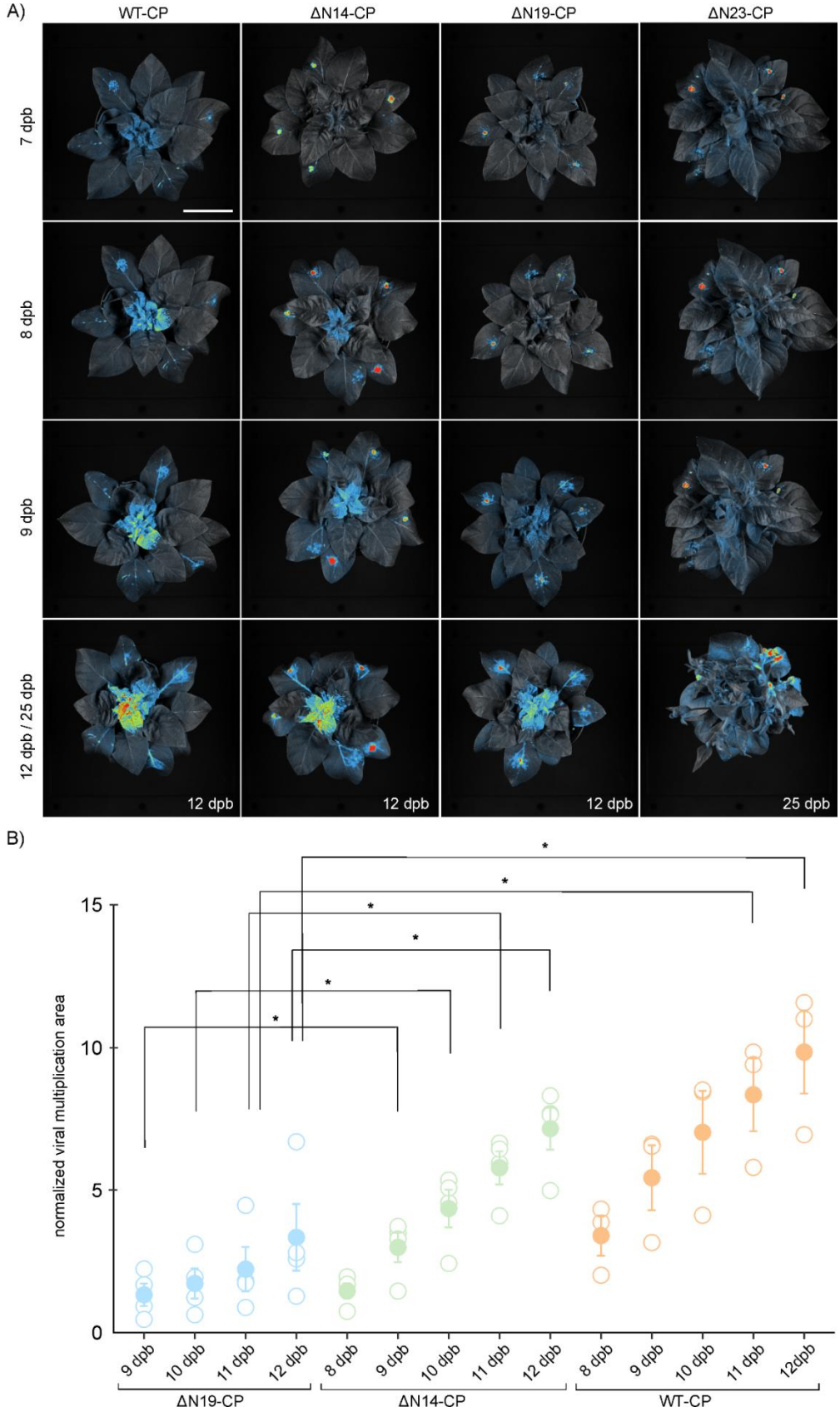
A)
WT-CP
ΔN14-CP
ΔN19-CP
ΔN23-CP
7 dpb
8 dpb
9 dpb
12 dpb / 25 dpb
12 dpb
12 dpb
12 dpb
25 dpb
B)
normalized viral multiplication area
15
10
5
0
9 dpb
10 dpb
11 dpb
12 dpb
8 dpb
9 dpb
10 dpb
11 dpb
12 dpb
8 dpb
9 dpb
10 dpb
11 dpb
12dpb
ΔN19-CP
ΔN14-CP
WT-CP

188 **Figure 3. Systemic viral spread of mutants is delayed similarly as cell-to-cell movement. (A)** Spatio-
189 temporal PVY distribution in *N. clevelandii* systemic tissue. Viral multiplication area was followed 7-12 and
190 25 days post bombardment (dpb), by using whole plant imaging system. Scale bar: 5 cm. **(B)** Quantification
191 of viral multiplication area in ROI in the *N. clevelandii* systemic tissue in total count per mutant in five
192 selected timepoints including 8-12 dpb. Since ΔN19-CP did not spread systemically at 8 dpi, normalized
193 viral multiplication area is not shown. Mean (represented with filled dot) and standard error are shown.
194 Individual measurements are shown as empty dots, representing normalized viral multiplication area.
195 Differences were statistically evaluated using Welch`s t test. Statistically significant differences ($p < 0.05$) are
196 marked with asterisk. Raw and normalized data, number of plants and statistics are specified in data S7.
197 Since ΔN26-CP is not capable of spreading systemically, it was not included in the analysis. Also ΔN23-CP
198 had such a delayed spread that it was not possible to do a quantification of viral multiplication area at 8 to 12
199 dpb (Fig. 3A).

200 Quantitative analysis of viral multiplication signal in systemic tissue confirmed that WT-CP achieved
201 the largest multiplication area, followed by ΔN14-CP and lastly ΔN19-CP in all observed time points
202 (Fig. 3 and data S7). When comparing ΔN14-CP and WT-CP, we observed a trend of slower spread
203 in case of ΔN14-CP, albeit not statistically significant (Fig. 3B and data S7). ΔN23-CP was not
204 included in the comparison, due to the considerable delay in the systemic spread exhibited by this
205 mutant (Fig. 3A), which made it difficult to measure the viral multiplication area. In conclusion,
206 systemic viral spread is abolished for ΔN26-CP, and decreasingly hampered in case of ΔN23-CP,
207 ΔN19-CP, while ΔN14-CP mutant is able to move similarly as WT-CP, albeit with a short delay.

208 **Substitution of serine with glycine on position 21 of CP N terminal region abolished PVY**
209 **cell-to-cell viral movement and virion assembly**

210 To pinpoint amino acids important for cell-to-cell virus movement, we generated point mutations in
211 the part of CP N terminal region that was observed as being important for viral movement (Figs. 1,
212 2 and 3). We point mutated charged residues Asp14, Glu18, potential phosphorylation site at Ser21
213 and 3D structure breakers Gly20 and Pro24. All, except Pro24, are highly conserved across
214 sequenced PVY strains. At position 24, 50% of PVY strains carries Pro and the others Ser (Fig S9).

Selected residues were changed to Ala (D14A, E18A, P24A), except for Ser21 where the sequence coding for Ala and Thr substitution was unstable in *E. coli*, thus we mutated it to Gly (S21G) and for Gly20, where we intentionally introduced Pro (G20P) to affect the fold of N terminal region (Fig. 4A).

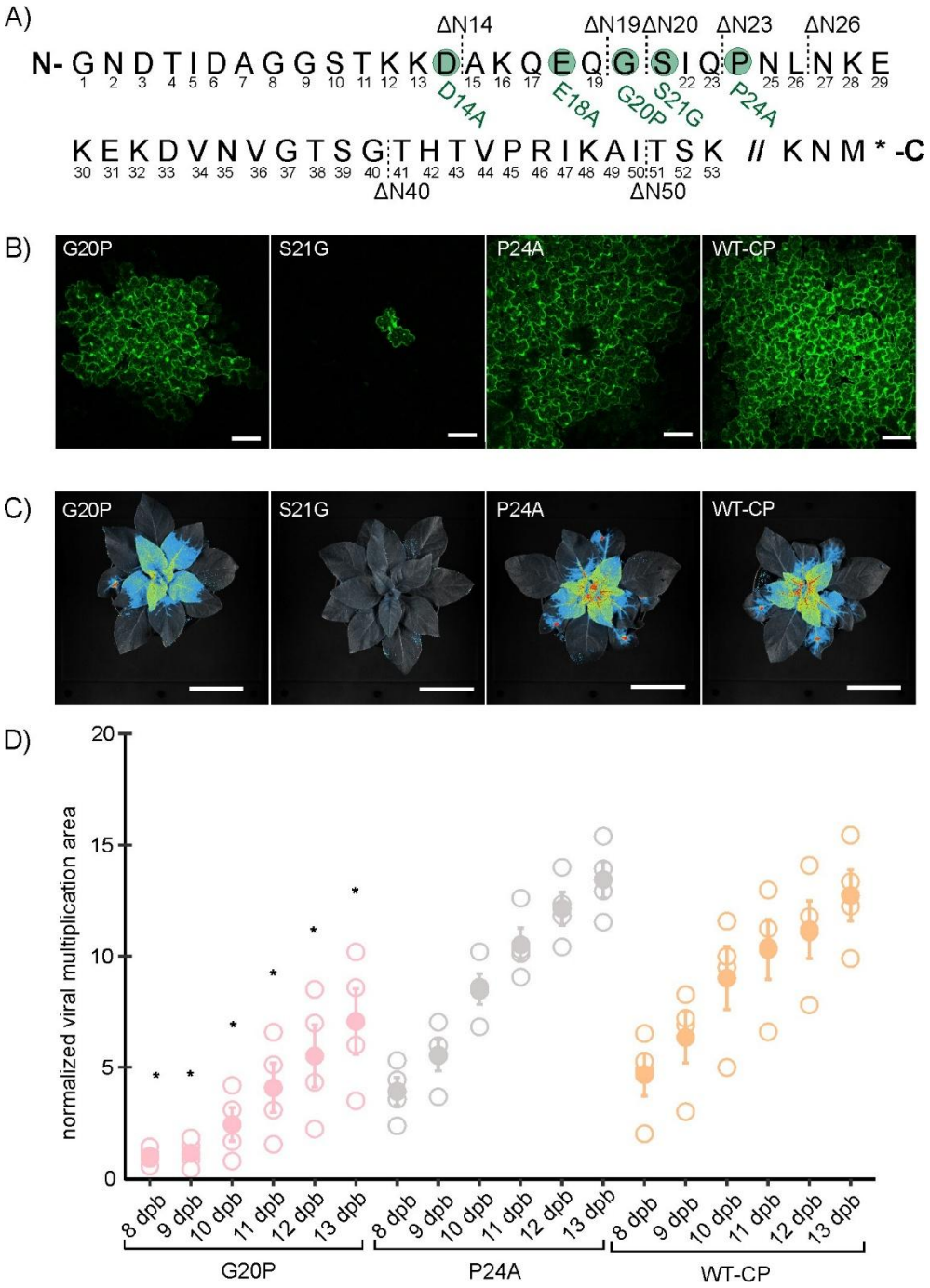

220

221 **Figure 4. Substitution of serine to glycine on position 21 of CP N terminal region abolished cell-to-**
222 **cell viral movement. (A)** Amino acid sequence of GFP tagged infectious clone PVY-N605(123) CP protein
223 with labeled constructed deletion and point mutants. The scheme presents mutants with deletions of 14
224 (ΔN14-CP), 19 (ΔN19-CP), 20 (ΔN20-CP), 23 (ΔN23-CP), 26 (ΔN26-CP), 40 (ΔN40-CP) or 50 (ΔN50-CP)
225 amino acids on CP N terminal region and mutants with point mutations including substitutions of negatively
226 charged aspartic acid to alanine on position 14 (D14A), negatively charged glutamic acid to alanine on
227 position 18 (E18A), glycine to proline on position 20 (G20P), serine to glycine on position 21 (S21G) and
228 proline to alanine on position 24 (P24A). **(B)** Confocal microscopy images showing viral cell-to-cell spread of
229 mutants G20P, S21G, P24A and WT-CP 5 dpb. Scale is 100 μm. **(C)** Spatio-temporal PVY distribution for
230 constructed point mutants G20P, S21G, P24A and WT-CP in *N. clevelandii* systemic tissue as observed by
231 whole plant imaging system 12 dpb. Scale is 5 cm. **(D)** Quantification of viral multiplication area in the upper
232 systemic leaves of bombarded *N. clevelandii* in 6 selected timepoints (8-13 dpb). Mean (represented with
233 filled dot) and standard error are shown. Individual measurements are shown as empty dots, representing
234 normalized viral multiplication area. Differences between analyzed point mutants were evaluated with
235 Welch`s t test. Statistically significant differences ($p<0.05$) between G20P mutant and WT-CP are
236 represented with asterisks (*), while there were no statistically observed differences between P24A and WT-
237 CP (see data S8 for all results of statistical testing). Vertical lines present all points except outliers. The
238 results were confirmed in additional experiments (Fig. S5 and data S9).

239 Viral cell-to-cell spread of mutants D14A, E18A and P24A was comparable to WT-CP (Fig. 4B and
240 S6). On the other hand, G20P mutant showed delayed cell-to-cell spread, while S21G mutant
241 remained limited to just single cells at all observed timepoints (Figs. 4B and S6).

242 Next, we performed whole plant imaging to study systemic viral spread of mutants (Figs. 4C and
243 S8). In accordance with the results of cell-to-cell movement, there were no statistically significant
244 differences in viral multiplication area in systemic tissue when comparing D14A, E18A or P24A with
245 WT-CP (Figs. 4D, S7, S5 and data S8, S9, S10, S11) at all observed timepoints. On the other hand,
246 the viral multiplication area of G20P in systemic tissue was statistically significantly lower compared
247 to WT-CP at all observed time points (Fig. 4D and data S8). As expected, S21G did not spread

248 systemically (Fig. 4C). Furthermore, viral assembly was confirmed with electron microscopy in all
249 constructed point mutants, with S21G as an exception, where only oligomeric rings were observed
250 (Supp. Fig. S10).

251 **Discussion**
252
253 The biological function of C and N terminal regions of PVY CP has already been initiated in our
254 previous study, where we hypothesized that N terminal amino acid residues are necessary for an
255 efficient cell-to-cell movement (17). Here we provide additional insights into the mechanism of PVY
256 spread by identifying the regions of PVY CP N terminal region that are important for efficient viral
257 cell-to-cell movement and systemic infection.

258 Despite the conserved flexible structure of potyviruses N terminal region of CP, there are notable
259 differences observed regarding its involvement in potyviral cell-to-cell and systemic movement. In
260 the case of zucchini yellow mosaic virus (ZYMV), deletion of the entire CP N terminal region did
261 not affect systemic infection (23). Similarly, a deletion of 6-50 amino acids in the CP N terminal
262 domain did not compromise TuMV cell to cell and systemic movement (19). On the other hand, in
263 tobacco etch potyvirus (TEV), CP N terminal region deletions of 5-29 amino acid residues delayed
264 cell-to-cell movement and prevented systemic spread (22). We observed inability to move cell-to-
265 cell for PVY when 40 or more amino acid residues were deleted from CP N terminal region (Fig.
266 1). However, shorter deletions in the range of 19 to 23 did not prevent systemic spread but resulted
267 in delayed systemic and cell-to-cell PVY movement (Figs. 2, B and C, 3B and data S4, S3 and
268 S7).The observed differences among potyviral species may stem from the high phylogenetic
269 divergence inherent to the genus, which at the CP level is, among other variations, observed as
270 different lengths and nucleotide variations in the N terminal region across different potyvirus species
271 (29, 23, 30, 31, 32). It is also well known that the potyvirus movement is facilitated by various
272 protein components, both from the virus and the host plant (33, 34, 35, 10, 11). In addition
273 potyviruses exhibit a divergent host range , majority of them being naturally limited to narrow host
274 range, such as TEV and ZYMV (36, 37), while TuMV stands out with its remarkably broad natural
275 host range (38). These features could also be contributing to the differences in the influence that

276 CP N terminal domain deletions have on the movement of different potyvirus species, because
277 different components involved in potyviral movement, viral and host, could be differently
278 compensating the effect of CP N terminal deletions.

279 The analysis of viral multiplication area revealed important insights into the cell-to-cell movement
280 dynamics of deletion mutants, as increasing number of deleted amino acid residues at CP N
281 terminal region resulted in slower cell-to-cell viral spread (Fig. 2, B and C). Furthermore, slower
282 cell-to-cell virus spread also impacted infection of systemic tissue (Fig. 3A). The connection
283 between cell-to-cell movement and systemic spread was expected, as the virus reaches the veins,
284 enters the veins and is transported in systemic tissue with a delay due to decelerated cell-to-cell
285 movement (39).

286 Results of several studies showed the role of charged amino acids in the CP core, C and N terminal
287 region of different potyviruses in cell-to-cell and systemic virus spread (20, 26, 40, 41). In contrast,
288 substitutions of charged amino acids in the CP N terminal region of PVY in our study (D14A and
289 E18A mutants) did not affect cell-to-cell spread (Fig. 4B). It was also reported (42) that aromatic
290 residues, located on the core CP region contribute to the formation of π-stackings that are
291 importantly involved in TVBMV and other potyvirus movement, since they maintain CP
292 accumulation by stabilizing α-helixes and β-sheets (43, 44). Our region of interest does not possess
293 aromatic amino acid residues, therefore we did not test this hypothesis.

294 However, we observed that replication of S21G mutant was limited to single cells (Fig. 4B). We
295 further checked and the intensity of replication of this mutant within this single cell was not affected
296 (Table S2). Interestingly, electron microscopy imaging showed impaired viral assembly, since only
297 oligomeric rings were observed (Supp Fig. S10). Correct viral particle assembly is however not
298 prerequisite for cell to cell movement as ΔN40 and ΔN50 mutants did assemble but still could not
299 move between cells (Figs. 1 and S10). We hypothesize that this might be due to loss of potential
300 phosphorylation site or disruption of N-terminus structure, due to introduction of glycine. Previous
301 studies suggested that posttranslational modifications such as phosphorylations have an important

302 role in viral cell-to-cell movement and virion assembly (45, 46). In potato virus A (PVA),
303 phosphorylation of Thr243 residue on CP C terminal region is crucial for PVA replication in planta
304 (21). Note that to confirm the hypothesis about role of phosphorylation of Ser21, we aimed to
305 replace Ser21 also with alanine and threonine, but the design of such point mutants was not
306 achievable, due to their instability in *E. coli*. It has been previously suggested that PVY cDNA is
307 unstable in *E. coli*. Stability of full length PVY plasmids was achieved by inserting introns into
308 putatively toxic genes but still for some mutants recombinations can occur (47).

309 Furthermore, we also showed the important role of the glycine on position 20 of CP N terminal
310 region in PVY cell-to-cell as well as systemic spread, since G20P mutant spreads slower than WT-
311 CP (Fig. 4 B, C and D). We hypothesize that exchanging Gly with Pro in G20P mutant increased
312 rigidity in the N terminal region. Consequently, the interaction of the CP with other host and viral
313 proteins in the cell may be impaired, resulting in the observed delay. Moreover, alignment of first
314 50 amino acid residues from PVY CP N terminal region across all PVY isolates, revealed a high
315 degree of conservation (at least 92,9%) at the mutated residues 20 (G20P) and 21 (S21G) across
316 all PVY isolates (Fig. S9), further supporting biological significance of these amino acids in PVY.

317 The results identifying crucial domains and amino acids of CP N terminal region in viral cell-to-cell
318 movement provided in our study are important basis to elucidate these complex processes,
319 particularly in most economically important viruses such as PVY.

320 **Materials and Methods**
321
322 **Plant material**

323 *N. clevelandii* plants were used to follow virus spread. Plants were grown from seeds and kept in
324 growth chambers under controlled conditions as described previously (48).

325 **Construction of PVY-N605(123)-GFP CP N-terminal deletion and point mutants**

326 As a template to construct mutants with deletions on the CP N terminal region, we used a GFP-
327 tagged infectious clone PVY-N605(123) (28). The GFP coding sequence was inserted between NIb
328 and CP coding sequences, flanked by protease target sequences, so that GFP would not bother
329 viral movement, since it is excised from the polyprotein as other viral proteins (28). Megaprimers
330 were designed in accordance with instructions prepared by (49). Detailed information about
331 mutagenic PCR reactions conditions and mixtures can be found in Text S1. After adding 4 µL of
332 DpnI enzyme, the mutagenesis mixtures were transformed into *E. coli* XL 10 Ultracompetent Cells
333 in accordance with manufacturer`s instructions (Agilent Technologies). Transformation mixtures
334 were plated on LB agar with ampicillin selection and incubated overnight at 37ºC. Transformants
335 were screened with colony PCR using PVY GFP_F and PVY uni_R primers (data S12) and
336 KAPA2G Robust HotStart Kit (Agilent Technologies). Prior bombardment, polyprotein and its
337 promoter in PVY-N605(123) lacking 50 and 14 amino acids on CP N-terminus were Sanger
338 sequenced (data S12). Additionally, restriction analysis was performed to confirm the correctness
339 of the PVY coding region.

340 **Biolistic bombardment**

341 Constructed PVY mutants and wild type plasmids were amplified in *E. coli*. Plasmids were then
342 isolated and coated onto gold microcarriers that were used for *N. clevelandii* bombardment using
343 a Helios® gene gun (Bio-Rad), as described by (49).

344

345

346 **Plant material sampling and RNA isolation**

347 Plant leaf samples were collected from bombarded *N. clevelandii* plants by excising 0,3 g plant
348 tissue near the bombardment site. Sampled plant material from bombarded *N. clevelandii* leaves
349 was homogenized in 700 µl of RNeasy kit RLT lysis buffer with FastPrep (MP Biomedicals) 1 min
350 6,5 m/s. Total RNA was isolated using RNeasy Plant Mini Kit (Qiagen). Residual DNA was digested
351 with deoxyribonuclease I (DNase I, Qiagen) in solution, using 1.36U DNase/µg RNA. Quality control
352 of isolated RNA was performed as described (48).

353 **RT-qPCR**

354 Relative PVY RNA concentration was determined by single-step quantitative RT-PCR (RT-qPCR;
355 AgPath-ID One-Step RT-PCR, Thermo FisherScientific) for the ΔN50-CP mutant, while two step
356 RT-qPCR was performed for other mutants. RNA was reverse transcribed with High-Capacity cDNA
357 Reverse Transcription Kit (Thermo Fisher Scientific) and analyzed by qPCR using FastStart
358 Universal Probe Master (Roche).

359 A qPCR assay targeting the PVY CP encoding region was used as a target gene, while the gene
360 encoding for cytochrome oxidase (COX) was used as reference gene. To avoid false positive
361 results plants bombarded with plasmid encoding for blue fluorescent protein, were sampled and
362 analyzed with our qPCR assay targeting PVY CP encoding region. RT-qPCR amplification program
363 and reaction composition mixtures were the same as previously described (28). Primers and
364 Probes details are listed in data S12.

365 After conducting RT-qPCR reactions, the QuantGenius software (50) was used for relative
366 quantification of PVY RNA using the standard curve approach. Data containing information about
367 the relative RNA quantity, was averaged for each group and then normalized to the lowest group
368 average number (data S1).

369

370

371 **RT-PCR**

372 One-step reverse transcription PCR (QIAGEN OneStep RT-PCR Kit) was performed to confirm that
373 the introduced mutations were maintained in the viral progeny of all constructed mutants. DNAse-
374 treated RNA, isolated from leaves according to the above protocol, was used as a template.
375 Mutated region was amplified with PVY-GFP_F and uniPVY_R primers (data S12). The purified
376 PCR products were sequenced (Sanger sequencing). For samples with a small amount of mutated
377 virus (ΔN50-CP, ΔN40-CP, S21G), an additional PCR (repliQa HiFi ToughMix; Quantabio) on
378 purified products was performed to amplify the mutated region in sufficient quantity.

379 **Confocal microscopy**

380 Cell-to-cell viral spread on upper side of bombarded *N. clevelandii* leaf discs, sampled with cork
381 borer, was observed under Leica TCS LSI confocal macroscope with Plan APO x5 and x20
382 objectives (Leica Microsystems, Wetzlar, Germany) at different time points (5-14 dpb), and Stellaris
383 5 confocal microscope with HC PL FLUOTAR x10 objective (Leica Microsystems, Wetzlar,
384 Germany) for studying point mutations at 5 dpb. The GFP emission was recorded after excitation
385 with 488 nm laser in the window between 505 and 530 nm and used as a direct measure of the
386 presence of metabolically active viruses in the observed tissue. Sampled discs were scanned
387 unidirectionally with scan speed of 400 Hz and frame average 1 or 2. For following the spread of
388 ΔN50-CP at 12 dpb, 5x and 20x objective were used (Fig. 1B), for ΔN40-CP and WT-CP at 5 and
389 10 dpb, 5x objective was used (Fig. 1B), while for following the spread of ΔN26-CP at 5-14 dpb and
390 ΔN23-CP, ΔN20-CP, ΔN19-CP, ΔN14-CP mutants and WT-CP at 5 dpb, 20x objective was used
391 (Fig. 1C and D). For each mutant we observed at least 3 plants.Images were processed using
392 LEICA LAS X software (Leica microsystems) to obtain maximum projections from z-stacks. Raw
393 confocal microscopy images were deposited on Zenodo (doi: 10.5281/zenodo.17177382).

394 **Transmission electron microscopy sample preparation**

395 Viral assembly was assessed with transmission electron microscopy (TEM) using negative staining
396 method. Tissue extracts were prepared from leaf discs, in which viral presence was previously

397 confirmed with confocal microscope, and then macerated in phosphate buffer (0.1 M, pH 6.8). 20
398 µL of extracts were applied to a grid for 5 minutes, blotted, washed, and stained with 1% (w/v) water
399 solution of uranyl acetate. Grids were observed by TEM TALOS L120 (Thermo Fisher Scientific)
400 operating at 100 kV or 120 kV. Micrographs were recorded using Ceta 16 M camera and software
401 Velox (Thermo Fisher Scientific). Raw electron microscopy images were deposited at Zenodo (doi:
402 10.5281/zenodo.17177382).

403

404 **Virus inoculation**

405 To more precisely examine cell-to-cell viral movement by whole plant imaging, we inoculated 3-4
406 weeks old *N. clevelandii* plants with inoculum prepared from systemic leaves of ΔN14-CP, ΔN19-
407 CP, ΔN23-CP and WT-CP-inoculated plants in which GFP signal was confirmed using whole plant
408 imaging system. Systemic leaves were ground in phosphate buffer (supplemented with PVP 10000)
409 in a plant material : buffer ratio of 1:4. Three bottom leaves of *N. clevelandii* plants were dusted
410 with carborundum powder and rubbed with the inoculum (1-3 drops of inoculum per leaf) which was
411 removed after 10 min by rinsing with tap water.

412 **Whole plant imaging**

413 Cell-to-cell and systemic viral spread throughout the plant was monitored using the Whole plant
414 imaging system Newton 7.0 BIO (Vilber) in bombarded and inoculated *N. clevelandii* plants. GFP
415 emission of GFP-tagged PVY clone was followed in 480 nm excitation channel and emission filter
416 F-550. Images were taken by EvolutionCapt edge software. For viral multiplication area analysis in
417 inoculated leaves, all three ΔN14-CP-, ΔN19-CP-, ΔN23-CP- and WT-CP-inoculated leaves of *N.*
418 *clevelandii* were imaged using exposure time 1 min 46 sec 700 msec, 10x10 field of view (FOV)
419 and 1331-1337 focus in 4 time points: 3 dpi a.m. and p.m. and 4 dpi a.m. and p.m. Measurements
420 for a.m. timepoint were carried out 9 a.m, while for p.m timepoint at 1 p.m. Four plants inoculated
421 with each mutant or WT-CP were imaged. For studying systemic viral spread, at least 3 *N.*
422 *clevelandii* plants bombarded with ΔN26-CP, ΔN23-CP, ΔN14-CP, ΔN19-CP- and WT-CP were

423 imaged, using 50 s exposure time, 20x20 FOV and focus in the range between 1871 and 1905 in
424 different time points (7-12 dpb). Note that *N. clevelandii* plants bombarded with ΔN26-CP and
425 ΔN23-CP were not taken into analysis, due to their inability or big delay in systemic movement. For
426 studying systemic viral spread of point mutations, at least three plants bombarded with constructed
427 point mutants were imaged at different time points (6-13 dpb) with exposure time 50 s and other
428 settings as for studying systemic viral spread of deletion mutants (see above). In case of
429 experiment with D14A and WT-CP at 13 dpb, exposure time was only 5 s to avoid saturation due
430 to a high signal. Raw images were deposited at Zenodo (doi: 10.5281/zenodo.17177382).

431

432 **Image analysis and signal quantification following whole plant imaging**

433 Viral multiplication area analysis on inoculated leaves and on upper systemic leaves were
434 performed using Kuant software (Vilber, France). In case of viral multiplication area, surfaces of
435 three viral multiplication areas per leaf were measured, while in case of viral multiplication area in
436 systemic leaves, total count of the virus affected area was measured. Total count is determined as
437 a sum of gray values within region of interest (systemic leaves, ROI) and is proportional to the
438 intensity and spread of the signal. All measured data from Kuant software were exported to Excel,
439 where total count in ROIs were averaged for each timepoint and subsequently normalized on the
440 lowest group average number. Normalized viral multiplication areas were statistically evaluated
441 using Welch`s t-test and were used for graphic representation.

Acknowledgments

We thank Živa Lengar for technical support and laboratory assistance, Dr. Maja Zagorščak and Dr. Angelika Vižintin for help with statistical analysis.

Author contributions

AC, KG and TL designed research; TMP, KS, AC, AV, MTŽ, KB, VL performed the research; AV, TL, TMP, KS, MTŽ, VL, KG, AC, analyzed the data; AV, TL, AC, KG, TMP, KS, MTŽ, IGA, MP, KB, VL contributed to the writing or revision of the article.

Competing interests

The authors declare no competing interests.

Data availability

Raw confocal microscopy and whole plant imaging system pictures were deposited at Zenodo and are openly available at doi: 10.5281/zenodo.17177382).

455 **References**
456

457 1. Scholthof KBG, Adkins S, Czosnek H, Palukaitis P, Jacquot E, Hohn T, Hohn B,
458 Saunders K, Candresse T, Ahlquist P, Hemenway C, Foster GD. Top 10 plant viruses in
459 molecular plant pathology. Molecular Plant Pathology. 2011; 12: 938-954.
460
461 2. Quenouille J, Vassilakos N, Moury B. Potato virus Y: A major crop pathogen that has
462 provided major insights into the evolution of viral pathogenicity. Molecular Plant
463 Pathology. 2013; 14(5):439-452.
464
465 3. Ivanov KI, Eskelin K, Lõhmus A, Mäkinen K. Molecular and cellular mechanisms
466 underlying potyvirus infection. Journal of General Virology. Society for General
467 Microbiology. 2014; 95: 1415-1429.
468

469 4. Olspert A, Chung BY, Atkins JF, Carr JP, Firth AE. Transcriptional slippage in the positive-
470 sense RNA virus family Potyviridae. EMBO Rep. 2015; 16(8): 995-1004.

471

472 5. Chung BY, Miller WA, Atkins JF, Firth AE. An overlapping essential gene in the
473 Potyviridae. Proc Natl Acad Sci U S A. 2008; 105(15):5897-902.
474
475
476 6. Yang X, Li Y, Wang A. Research Advances in Potyviruses: From the Laboratory Bench to
477 the Field. Annu. Rev. Phytopathol. 2021; 59: 1-29.
478
479 7. Benitez-Alfonso Y, Faulkner C, Ritzenthaler C, Maule AJ. Plasmodesmata: Gateways to
480 Local and Systemic Virus Infection. MPMI. 2010; 23(11):1403-1412.
481
482
483 8. Folimonova SY, Tilsner J. Hitchhikers, highway tolls and roadworks: the interactions of
484 plant viruses with the phloem. Current Opinion in Plant Biology. 2018; 43: 82-88.
485
486 9. Reagan BC, Burch-Smith TM. Viruses reveal the secrets of plasmodesmal cell biology.
487 Molecular Plant-Microbe Interactions. 2020; 33: 26-39.
488
489
490 10. Revers F, García JA. Molecular biology of potyviruses. Advances in Virus Research.
491 2015; 92: 101-199.
492
493 11. Xue M, Arvy N, German-Retana S. The mystery remains: How do potyviruses move
494 within and between cells? Molecular Plant Pathology. 2023; 24: 1560-1574.
495 12. Wei T, Zhang C, Hong J, Xiong R, Kasschau KD, Zhou X, Carrington JC, Wang A.
496 Formation of complexes at plasmodesmata for potyvirus intercellular movement is
497 mediated by the viral protein P3N-PIPO. PLoS Pathogens. 2010; 6: e1000962.
498
499 13. Rojas MR, Zerbini FM, Allison RF, Gilbertson RL, Lucas WJ. Capsid Protein and Helper
500 Component-Proteinase Function as Potyvirus Cell-to-Cell Movement Proteins. Vol. 237,
501 Virology. 1997; 237: 283-295.
502

14. Navarro JA, Sanchez-Navarro JA, Pallas V. Key checkpoints in the movement of plant viruses through the host. In: Advances in Virus Research. 2019; 104: 1-64.

15. Mäkinen K, Hafrén A. Intracellular coordination of potyviral RNA functions in infection. Vol. 5, Frontiers in Plant Science. 2014; 5: 110.

16. Zamora M, Méndez-López E, Agirrezabala X, Cuesta R, Lavín JL, Amelia Sánchez-Pina M, Aranda MA, Valle M. Potyvirus virion structure shows conserved protein fold and RNA binding site in ssRNA viruses. Sci. Adv. 2017; 3: eaao2182.

17. Kežar A, Kavčič L, Polák M, Nováček J, Gutiérrez-Aguirre I, Žnidarič MT, Coll A, Stare K, Gruden K, Ravnikar M, Pahovnik D, Žagar E, Merzel F, Anderluh G, Podobnik M. Structural basis for the multitasking nature of the potato virus Y coat protein. Sci. Adv. 2019; 5: eaaw3808.

18. Cuesta R, Yuste-Calvo C, Gil-Cartón D, Sánchez F, Ponz F, Valle M. Structure of Turnip mosaic virus and its viral-like particles. Sci Rep. 2019; 9: 15396.

19. Dai Z, He R, Bernards MA, Wang A. The cis-expression of the coat protein of turnip mosaic virus is essential for viral intercellular movement in plants. Mol Plant Pathol. 2020; 21(9):1194-1211.

20. Seo JK, Vo Phan MS, Kang SH, Choi HS, Kim KH. The charged residues in the surface-exposed C-terminus of the Soybean mosaic virus coat protein are critical for cell-to-cell movement. Virology. 2013; 446: 95-101.

21. Lõhmus A, Hafrén A, Mäkinen K. Coat Protein Regulation by CK2, CPIP, HSP70, and CHIP Is Required for Potato Virus A Replication and Coat Protein Accumulation. J Virol. 2017; 91: e01316-16.

22. Dolja VV, Haldeman R, Robertson NL, Dougherty WG, Carrington JC. Distinct functions of capsid protein in assembly and movement of tobacco etch potyvirus in plants. EMBO Journal. 1994; 13(6):1482-1491.

23. Arazi T, Shiboleth YM, Gal-On A. A Nonviral Peptide Can Replace the Entire N Terminus of Zucchini Yellow Mosaic Potyvirus Coat Protein and Permits Viral Systemic Infection. J Virol. 2001; 75(14): 6329-6336.

24. Kimalov B, Gal-On A, Stav R, Belausov E, Arazi T. Maintenance of coat protein N-terminal net charge and not primary sequence is essential for Zucchini yellow mosaic virus systemic infectivity. Journal of General Virology. 2004; 85(11): 3421-3430.

25. Tatineni S, Kovacs F, French R. Wheat streak mosaic virus Infects Systemically despite Extensive Coat Protein Deletions: Identification of Virion Assembly and Cell-to-Cell Movement Determinants. J Virol. 2014; 88(2):1366-1380.

26. Tatineni S, French R. The C-terminus of Wheat streak mosaic virus coat protein is involved in differential infection of wheat and maize through host-specific long-distance transport. Molecular Plant-Microbe Interactions. 2014; 27(2): 150-152.

27. Tatineni S, Elowsky C, Graybosch RA. Wheat streak mosaic virus coat protein deletion mutants elicit more severe symptoms than wild-type virus in multiple cereal hosts. Molecular Plant-Microbe Interactions. 2017; 30(12): 974-983.

28. Lukan T, Županič A, Mahkovec Povalej T, Brunkard JO, Kmetič M, Juteršek M, Baebler Š, Gruden K. Chloroplast redox state changes mark cell-to-cell signaling in the hypersensitive response. New Phytologist. 2023; 237(2): 548-562.

29. Yuste-Calvo C, Ibort P, Sánchez F, Ponz F. Turnip Mosaic Virus Coat Protein Deletion Mutants Allow Defining Dispensable Protein Domains for 'in Planta' eVLP Formation. Viruses. 2020;12(6): 661.

30. Voloudakis AE, Malpica CA, Aleman-Verdaguer ME, Stark DM, Fauquet CM, Beachy RN. Structural characterization of Tobacco etch virus coat protein mutants. Arch Virol. 2004; 149(4): 699-712.

31. Gibbs A, Ohshima K. Potyviruses and the digital revolution. Annu Rev Phytopathol. 2010; 48: 205-223.

32. Gibbs AJ, Hajizadeh M, Ohshima K, Jones RAC. The potyviruses: An evolutionary synthesis is emerging. Viruses. 2020; 22: 132.

33. Ala-Poikela M, Rajamäki ML, Valkonen JPT. A Novel Interaction Network Used by Potyviruses in Virus-Host Interactions at the Protein Level. Viruses. 2019;11(12): 1158.

34. Martínez F, Rodrigo G, Aragonés V, Ruiz M, Lodewijk I, Fernández U, Elena SF, Daròs JA. Interaction network of tobacco etch potyvirus NIa protein with the host proteome during infection. BMC Genomics. 2016; 17: 87.

35. Vijayapalani P, Maeshima M, Nagasaki-Takekuchi N, Miller WA. Interaction of the trans-frame potyvirus protein P3N-PIPO with host protein PCaP1 facilitates potyvirus movement. PLoS Pathog. 2012; 8(4): e1002639.

36. García-Arenal F, Fraile A. Trade-offs in host range evolution of plant viruses. Plant Pathology. 2013; 62: 2-9.

37. Desbiez C, Lecoq H. Zucchini yellow mosaic virus. Plant Pathology. 1997; 46: 809-829.

38. Li G, Lv H, Zhang S, Zhang S, Li F, Zhang H, Qian W, Fang Z, Sun R. TuMV management for brassica crops through host resistance: retrospect and prospects. Plant Pathology. 2019; 68: 1035-1044.

605
606 39. Wang A. Dissecting the Molecular Network of Virus-Plant Interactions: The Complex
607 Roles of Host Factors. Annual Review of Phytopathology. 2015; 53: 45-66.
608
609
610 40. Atreya PL, Lopez-Moya JJ, Chu M, Atreya CD, Pirone TP. Mutational analysis of the coat
611 protein N-terminal amino acids involved in potyvirus transmission by aphids. J Gen Virol.
612 1995; 76: 265-70.
613
614 41. López-Moya JJ, Pirone TP. Charge changes near the N terminus of the coat protein of
615 two potyviruses affect virus movement. J Gen Virol. 1998; 79: 161-5.
616
617
618 42. Yan ZY, Xu XJ, Fang L, Geng C, Tian YP, Li XD. Multiple aromatic amino acids are
619 involved in potyvirus movement by forming π-stackings to maintain coat protein
620 accumulation. Phytopathol Res. 2021; 3:10.
621
622 43. Salonen LM, Ellermann M, Diederich F. Aromatic rings in chemical and biological
623 recognition: energetics and structures. Angew Chem Int Ed Engl. 2011; 50(21): 4808-42.
624 44. Chatterjee KS, Tripathi V, Das R. A conserved and buried edge-to-face aromatic
625 interaction in small ubiquitin-like modifier (SUMO) has a role in SUMO stability and
626 function. J Biol Chem. 2019; 294(17): 6772-6784.
627
628 45. Ivanov KI, Puustinen P, Gabrenaite R, Vihinen H, Rönnstrand L, Valmu L, Kalkkinen N,
629 Mäkinen K. Phosphorylation of the potyvirus capsid protein by protein kinase CK2 and its
630 relevance for virus infection. Plant Cell. 2003; 15(9):2124-39.
631
632
633 46. Hervás M, Navajas R, Chagoyen M, García JA, Martínez-Turiño S. Phosphorylation-
634 Related Crosstalk Between Distant Regions of the Core Region of the Coat Protein
635 Contributes to Virion Assembly of Plum Pox Virus. Mol Plant Microbe Interact. 2020;
636 33(4): 653-667.
637
638 47. Bukovinszki A, Götz R, Johansen E, Maiss E, Balázs E. The role of the coat protein
639 region in symptom formation on Physalis floridana varies between PVY strains. Virus
640 Res. 2007; 127: 122-125.
641
642
643 48. Baebler Š, Krečič-Stres H, Rotter A, Kogovšek P, Cankar K, Kok EJ, Gruden K, Kovac M,
644 Zel J, Pompe-Novak M, Ravnikar M. PVY(NTN) elicits a diverse gene expression
645 response in different potato genotypes in the first 12 h after inoculation. Mol Plant Pathol.
646 2009; 10(2): 263-275.
647
648 49. Stare K, Coll A, Gutiérrez-Aguirre I, Žnidarič MT, Ravnikar M, Kežar A, Kavčič L,
649 Podobnik M, Gruden K. Generation and in Planta Functional Analysis of Potato Virus Y
650 mutants. Bio Protoc. 2020; 10: e3692.
651
652
653 50. Baebler Š, Svalina M, Petek M, Stare K, Rotter A, Pompe-Novak M, Gruden K.
654 QuantGenius: Implementation of a decision support system for qPCR-based gene
655 quantification. BMC Bioinformatics. 2017; 18(1): 276.

51. Kogovšek P, Gow L, Pompe-Novak M, Gruden K, Foster GD, Boonham N, Ravnikar M, Single-step RT real-time PCR for sensitive detection and discrimination of Potato virus Y isolates. J Virol. 2008; 149: 1-11.

52. Weller SA, Elphinstone JG, Smith NC, Boonham N, Stead DE, Detection of Ralstonia solanacearum strains with a quantitative, multiplex, real-time, fluorogenic PCR (TaqMan) assay. Appl. Environ. Microbiol. 2000; 66: 2853-2858.

Supporting Information for

Functionality of potato virus Y coat protein in cell-to-cell movement dynamics is defined by its N terminal region

Anže Vozelj[1,2*], Tjaša Mahkovec Povalej[1], Katja Stare[1], Magda Tušek Žnidarič[1], Katarina Bačnik[1], Valentina Levak[1,2], Ion Gutiérrez-Aguirre[1], Marjetka Podobnik[3], Kristina Gruden[1], Anna Coll[1]†, Tjaša Lukan[1]†[*]

* Corresponding authors. Email: anze.vozelj@nib.si, tjasa.lukan@nib.si

This PDF file includes:

Supplementary Text S1. Construction of PVY-N605(123)- GFP CP N-terminal mutants
Fig. S1. ΔN50-CP ΔN40-CP viral replication.
Fig. S2. Viral replication ΔN26-CP.
Fig. S3. ΔN19-CP_ΔN14-CP_WT-CP cell-to-cell spread dynamics.
Fig. S4. ΔN26-CP inability of systemic spread
Fig. S5. Independent experiment for point mutants G20P, P24A and WT-CP to check viral abundance.
Fig. S6. Cell-to-cell viral spread of D14A, E18A, G20P, S21G and P24A point mutants.
Fig. S7. Virus abundance D14A, E18A, WT-CP.
Fig. S8. Point mutants systemic spread.
Fig. S9. Alignment of first 50 amino acid residues from the PVY N terminal region across all PVY isolates.
Fig. S10. Transmission electron microscopy (TEM) micrographs of deletion and point mutants.
Table S1. ΔN26-CP viral limitation on single cells or cell-to-cell spread.
Table S2. Replication efficiency of ΔN40-CP and S21G mutant is the same as the one of WT-CP PVY

699 **Supporting Information Text S1. Construction of PVY-N605(123)- GFP CP N-terminal**
700 **mutants.**

701 Mutants were prepared with mutagenic PCR using QuikChange II XL Site-Directed Mutagenesis
702 Kit (Agilent Technologies). As a template previously constructed GFP infectious clone PVY-
703 N605(123) was used (28). The megaprimers were synthesized using the N-terminal region
704 sequence of GFP tagged PVY-N605(123) plasmid, according to defined guidelines (49). All
705 megaprimers used in the study are listed in data S12. Mutagenic touchdown PCR reaction
706 program with the following reaction mixture in the final volume of 25 µL were the same for all
707 generated mutants according to previously published protocol for generation of PVY deletion
708 mutants (49), with minor modifications listed below.

Component	Final concentration	Volume [µL]
10x reaction buffer	1x	2,5
dNTP mix	200 µM	0,5
forward megaprimer	0,5 µM	1,25
reverse megaprimer	0,5 µM	1,25
QuikSolution	/	1,5
PVY-N605(123)	200 ng	1,2
PfuUltra HF DNA polymerase	/	1

709

Temperature	Time	Step
92ºC	2 min	hold
92ºC	50 s	
65ºC to 55ºC	50 s	10cycles
68ºC	30 min*	

92ºC	50 s	
55ºC	50 s	8 cycles
68ºC	30 min*	
68ºC	60 min	hold

710

711

712 After amplification, 4 µL of DpnI enzyme (Agilent Technologies) was added to the mutagenesis
713 reaction mixture, following 2h on 37ºC incubation. Following DpnI digestion, 2 µL of mutagenesis
714 mixture was used for transformation into *E. coli* XL-10 Gold Ultracompetent Cells (Agilent
715 Technologies). We used 45 µL cell aliquot supplemented with 2 µL of β-mercaptoethanol for the
716 standard heat-shock transformation protocol in accordance with the manufacturer's instructions
717 (Agilent Technologies). Transformation mixtures were plated on LB agar containing ampicillin and
718 incubated overnight at 37ºC. Transformants were analyzed with colony PCR using primers PVY
719 GFP_F and PVY uni_R with KAPA2G Robust HotStart Kit (Agilent Technologies) with the
720 following 10 µL reaction mixture and cycling conditions stated below.

721

722

Component	**Final concentration**	**Volume [µL]**
5x Buffer B	1x	2
10 mM dNTP	200 µM	0,2
10 µM PVY GFP_F	300 nM	0,3
10 µM PVY uni_R	300 nM	0,3
5 U/µL KAPA2G polymerase	0,3 U	0,06
Colony suspension	/	1
H20		6,14

Temperature	Time	Step
95 °C	10min	Hold
95 °C	30 s	
55 °C	15 s	30 cycles
72 °C	1 min	
72 °C	5 min	Hold

723 Sanger sequencing, using the same primers as for the colony PCR, of positive colonies was
724 performed to confirm correct sequence of the PVY coding part.
725
726 Designed mutants PVY-N605(123)-GFP with desired mutations were amplified in One Shot®
727 TOP10 *E. coli* and 50 µg of constructed plasmid mutants were isolated from overnight cultures
728 using GenElute Plasmid MiniPrep Kit (Sigma-Aldrich). Isolated plasmids were subsequently used
729 to coat 6.25 mg of gold microcarriers (0,6 µm) to prepare gene gun bullets according to the
730 manufacturers protocol and were used for *Nicotiana clevelandii* bombardment using a
731 Helios®gene gun (Bio-Rad) at 200 psi (49).
732

733 **Supporting figures and tables**

734

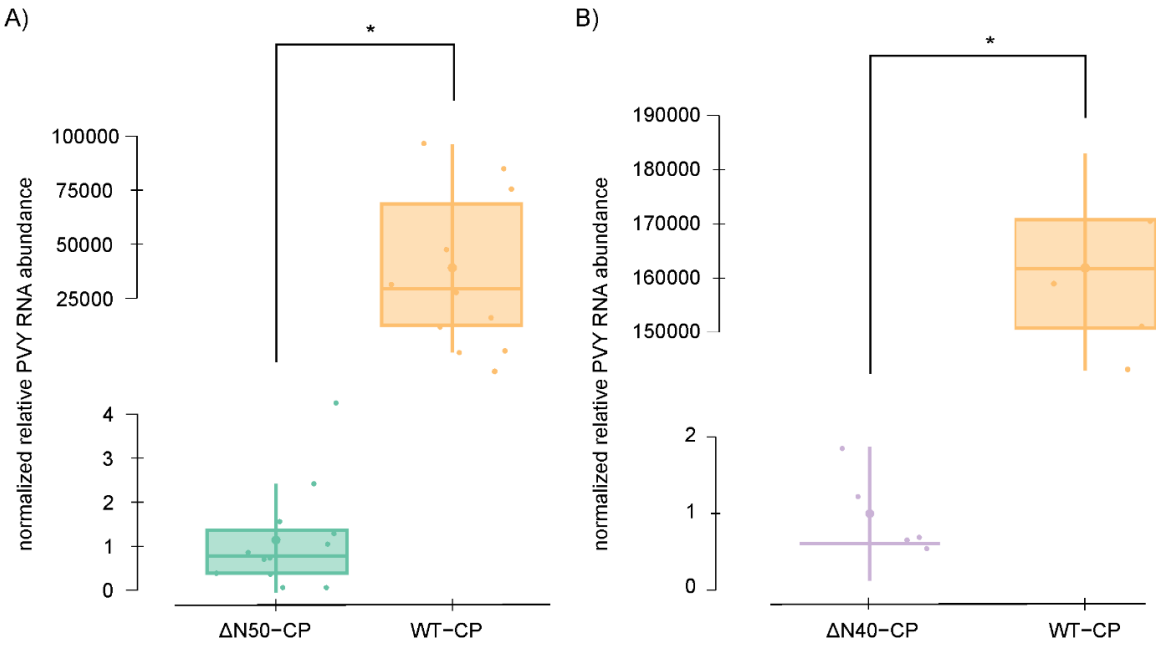

735
736

737 **Fig. S1. ΔN50-CP ΔN40-CP viral replication**. Normalized relative PVY RNA abundance in
738 bombarded *N. clevelandii* leaves for constructed PVY mutants lacking 50 (ΔN50-CP) (A) and 40
739 (ΔN40-CP) (B) amino acids at CP N-terminus. Results were obtained 14 days post bombardment
740 (dpb). Non-mutated infectious clone (WT-CP) was used as a control. Data normalization was
741 performed as described in data S1. Results are presented as boxplots with normalized relative
742 PVY RNA abundance for each sample shown as dots. Differences between ΔN50-CP and WT-CP
743 and between ΔN50-CP and WT-CP were statistically evaluated using Welch's t test. Statistically
744 significant differences (p<0,05) are marked with an asterisk (*). Vertical lines present all points
745 except outliers.

746

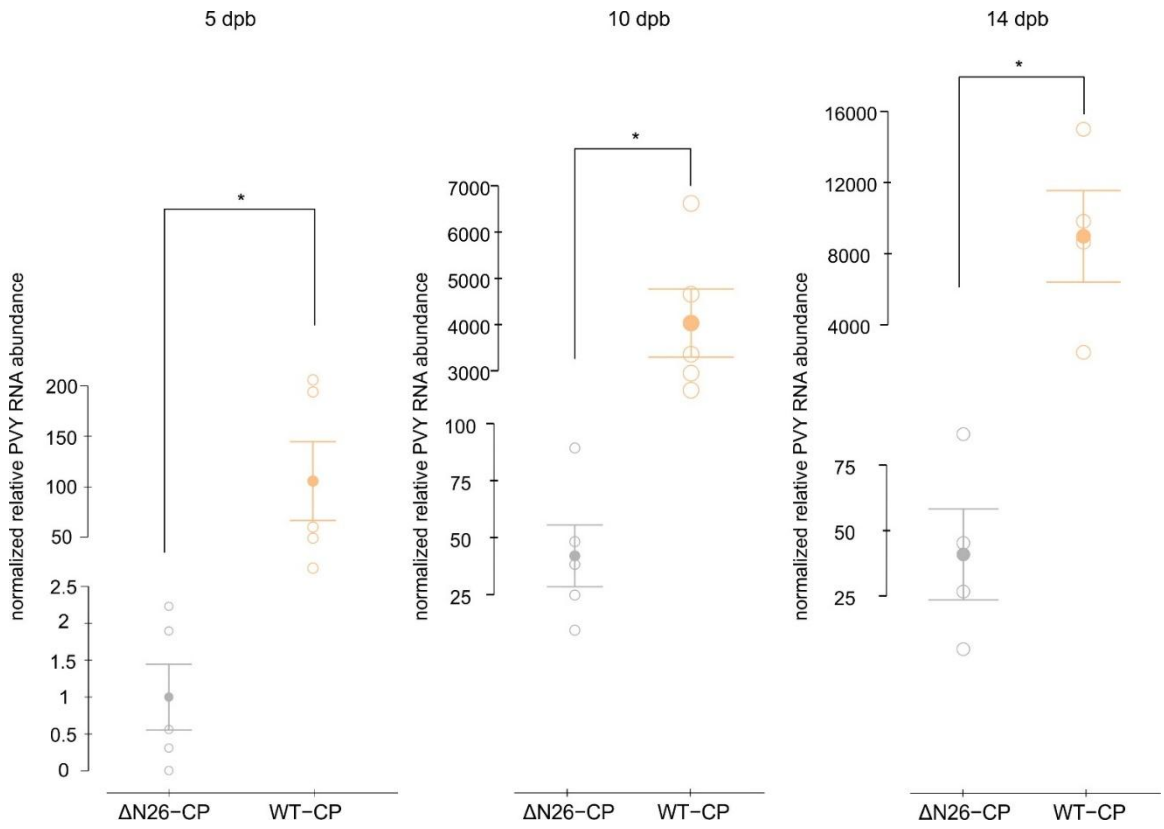

Fig. S2. Viral replication ΔN26-CP. Normalized relative PVY RNA abundance in bombarded *N. clevelandii* leaves for constructed PVY mutant lacking 26 amino acids residues, in three timepoints including 5, 10 and 14 dpb (from left to right). Non-mutated infectious clone (WT-CP) was used as a control. Data normalization was performed as described in data S1. Results are presented as mean (represented with filled dot) and standard error. Individual measurements are shown as empty dots, representing normalized relative PVY RNA abundance. Differences between constructed deletion mutants and WT-CP were statistically evaluated using Welch's t test. Statistically significant differences (p<0,05) are marked with an asterisk (*). Note that the scales are different between time points.

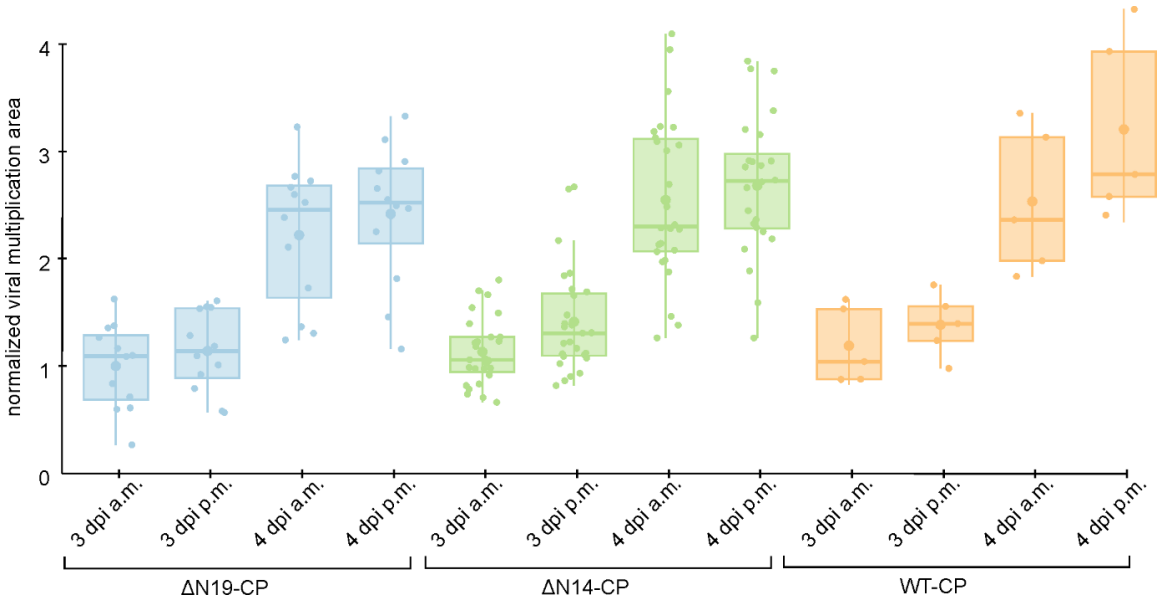

Fig. S3. N19-CP_ΔN14-CP_WT-CP cell-to-cell spread dynamics. Viral cell-to-cell spread dynamics was quantified with normalized viral multiplication analysis as described in Materials and methods. Results are presented as boxplots for tested mutants ΔN19-CP, ΔN14-CP and WT-CP in 4 tested timepoints including 3 dpi a.m., 3 dpi p.m., 4 dpi a.m. and 4 dpi p.m., where dots are representing normalized viral multiplication area as described in data S5. Differences were statistically evaluated using Welch`s t test. Vertical lines present all points except outliers. The differences were not statistically significant, due to autofluorescence of trichomes which resulted in saturated pixels.

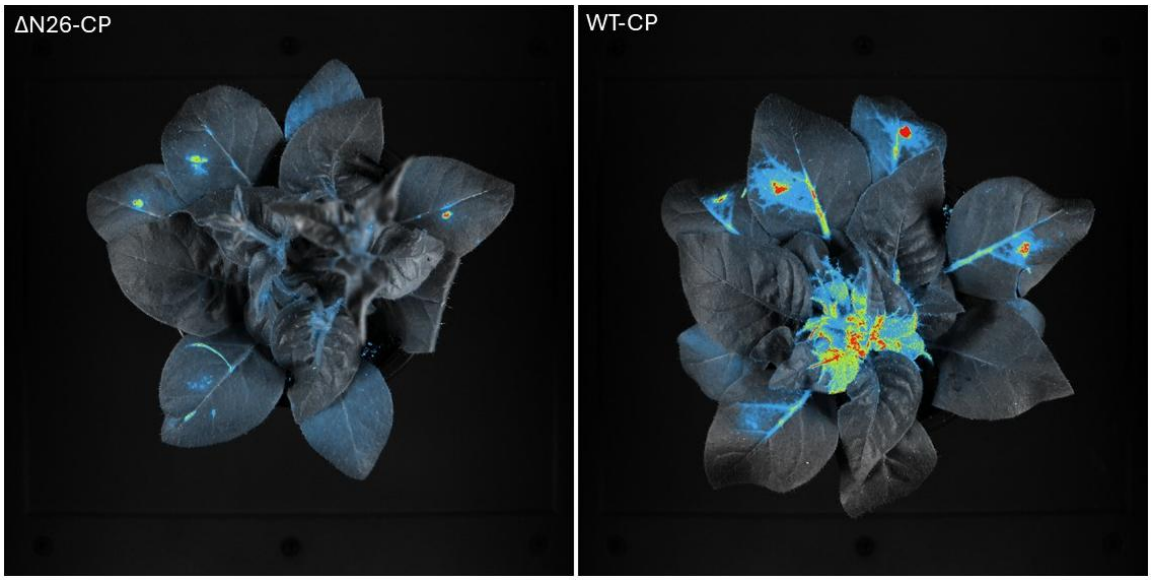

Fig. S4. ΔN26-CP inability of systemic spread. Viral systemic spread was abolished in ΔN26-CP mutant (left) in comparison to non mutated WT-CP, where systemic spread occurred (right). Pictures taken 12 dpb.

775

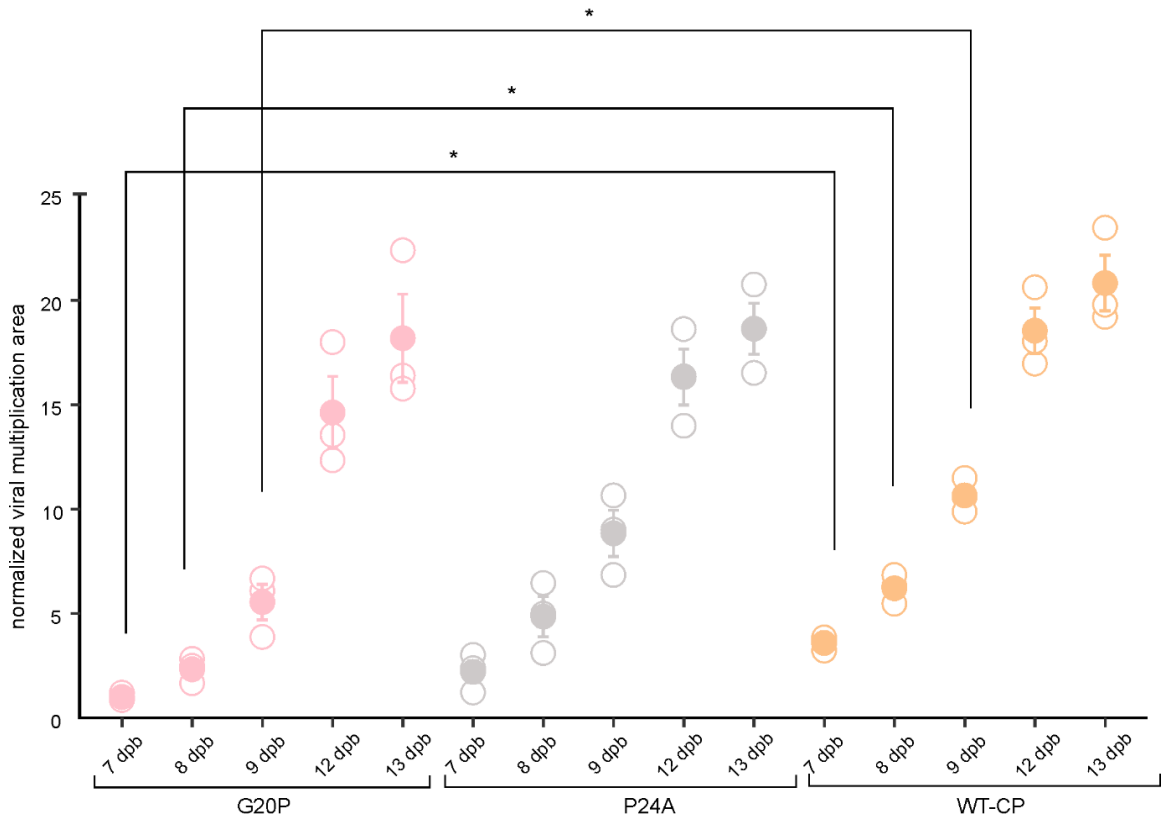

776

777 **Fig. S5. Independent experiment for point mutants G20P, P24A and WT-CP to check viral**
778 **abundance.** Quantification of virus abundance in the upper leaves of bombarded *N. clevelandii*
779 expressed as total count per mutant 7, 8, 9, 12 and 13 dpb with exposure time 50 s (A). Other
780 measurements settings are the same as stated in Materials and methods. Mean (represented
781 with filled dot) and standard error are shown. Individual measurements are shown as empty dots,
782 representing normalized viral multiplication area. Statistically significant difference in normalized
783 viral multiplication area between mutants was evaluated by Welch`s t test. Statistically significant
784 differences (p<0,05) are demarked with an asterisk (*). Raw and normalized data, number of
785 plants and results of statistical analysis are specified in data S9. Note that there was no
786 statistically significant difference between G20P and WT-CP at 12 and 13 dpb due to signal
787 oversaturation due to high exposure time (50 s).

788 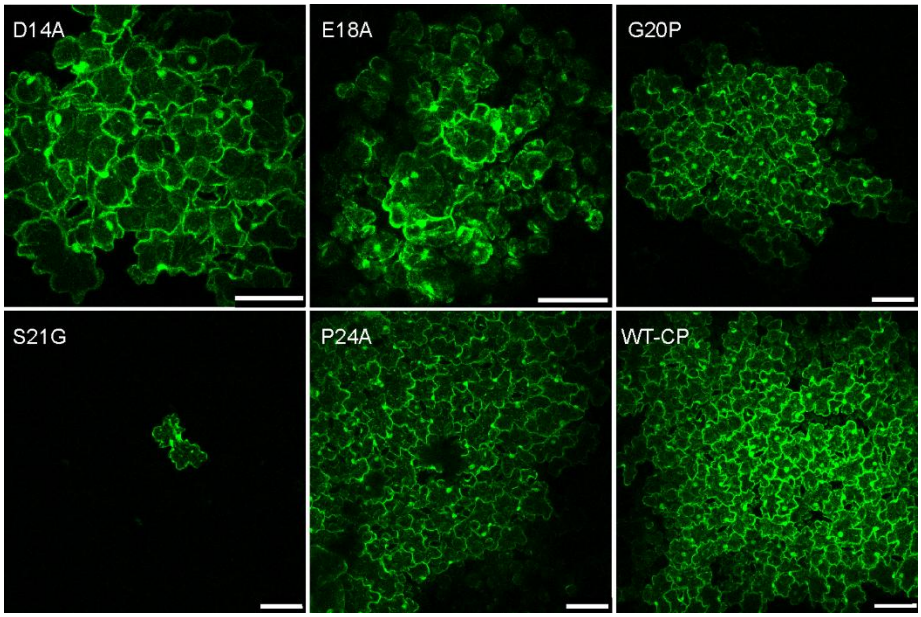

789 **Fig. S6. Cell-to-cell viral spread of D14A, E18A, G20P, S21G and P24A point mutants.**

790 Confocal microscopy images showing viral cell-to-cell spread of D14A, E18A, G20P, S21G, P24A

791 point mutants and WT-CP 5 dpb. Note that there we have comparisons of D14A and E18A point

792 mutants with the others (G20P, S21G, P24A) already included in the article main text (Fig. 4B).

793 Other confocal microscopy settings are specified in Materials and methods.

794

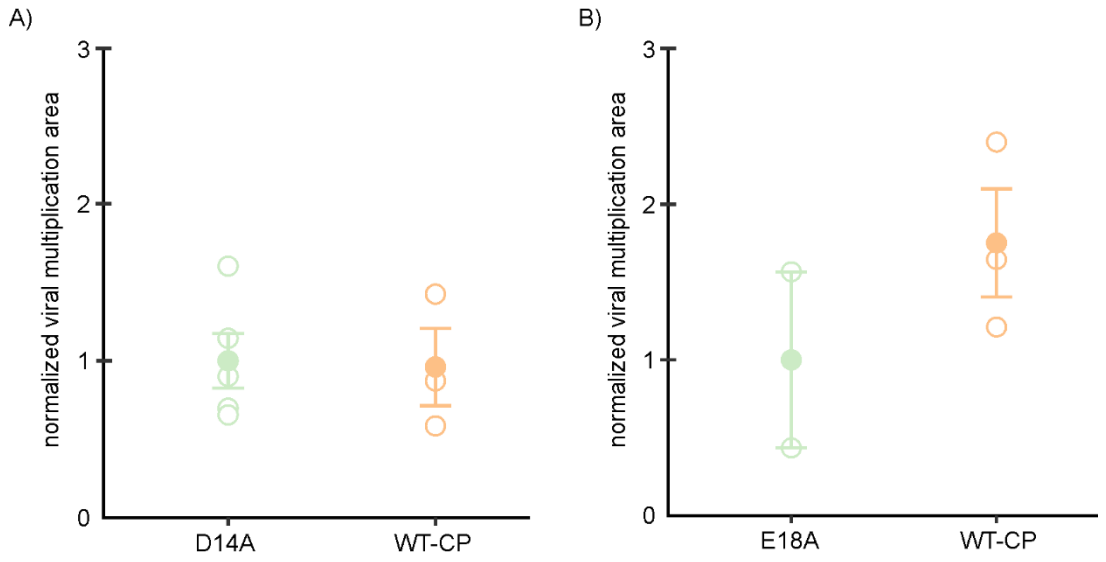

Fig. S7. Virus abundance D14A, E18A, WT-CP. Quantification of virus abundance in the upper leaves of bombarded *N. clevelandii* expressed as total count per mutant for D14A mutant 7 dpb with exposure time 50s (A) and (B) for E18A mutant 7 dpb with exposure time 50 (s). Other measurements settings are the same as stated in Materials and methods. Mean (represented with filled dot) and standard error are shown. Individual measurements are shown as empty dots, representing normalized viral multiplication area. There was no statistically significant difference in normalized viral multiplication area between mutants evaluated by Welch`s t test. Raw and normalized data, number of plants and results of statistical analysis are specified in data S10 and S11).

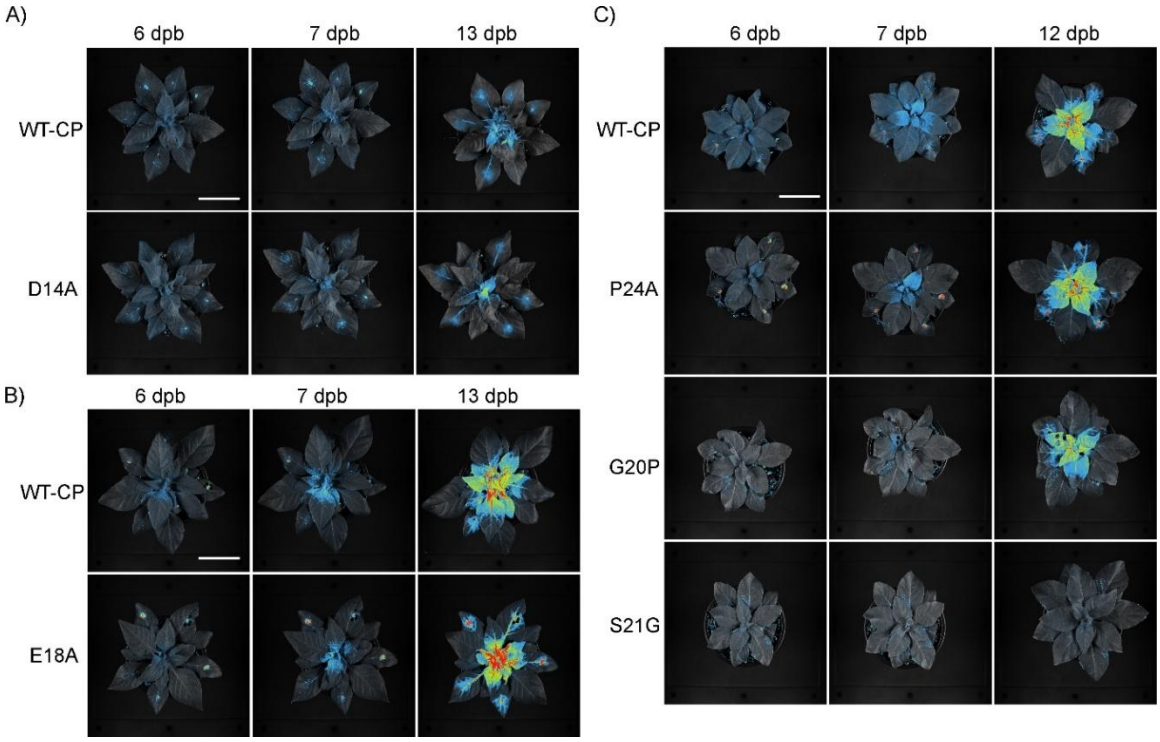

Fig. S8. Point mutants systemic spread. Spatio-temporal PVY distribution in *N. clevelandii* systemic tissue using whole plant imaging system. Systemic spread of constructed point mutants was followed 6 dpb, 7 dpb and 13 dpb in case of D14A (A) and E18A (B), while systemic spread of P24A, G20P and S21G. (C) was followed 6 dpb, 7 dpb and 12 dpb. Note that pictures for P24A, S21G and WT-CP 12 dpb are the same as in the main text (Fig. 4C). Imaging settings are specified in Materials and methods. Plants were imaged with exposure time 50 s. In case of D14A and WT-CP at 13 dpb, exposure time was 5 s to avoid oversaturation due to a higher signal.

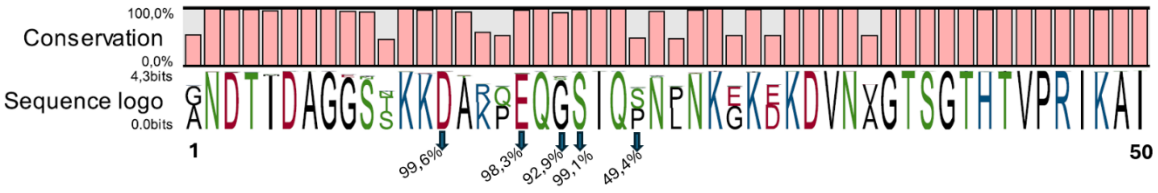

Fig. S9 Alignment of first 50 amino acid residues from the PVY N terminal region across all PVY isolates. To assess the conservation of mutated amino acid residues D14A, E18A, G20P, S21G and P24A, we performed multiple sequence alignment of the first 50 amino acid residues of the PVY coat protein, using CLC Genomics Workbench 25 (QIAGEN, Hilden, Germany) and pairwise sequence alignment. Note that for the multiple alignment analysis, only complete sequences containing the first 50 amino acid residues of the PVY coat protein N terminal region were included, as this region corresponds to our engineered deletion and point mutants. Altogether 2112 sequences were obtained from NCBI Virus database. Sequence logo represents the amino acid sequence conservation in the mutated region with arrows showing the conservation percentage of each point mutated amino acid (D14A, E18A, G20P, S21G, P24A) across all obtained sequences.

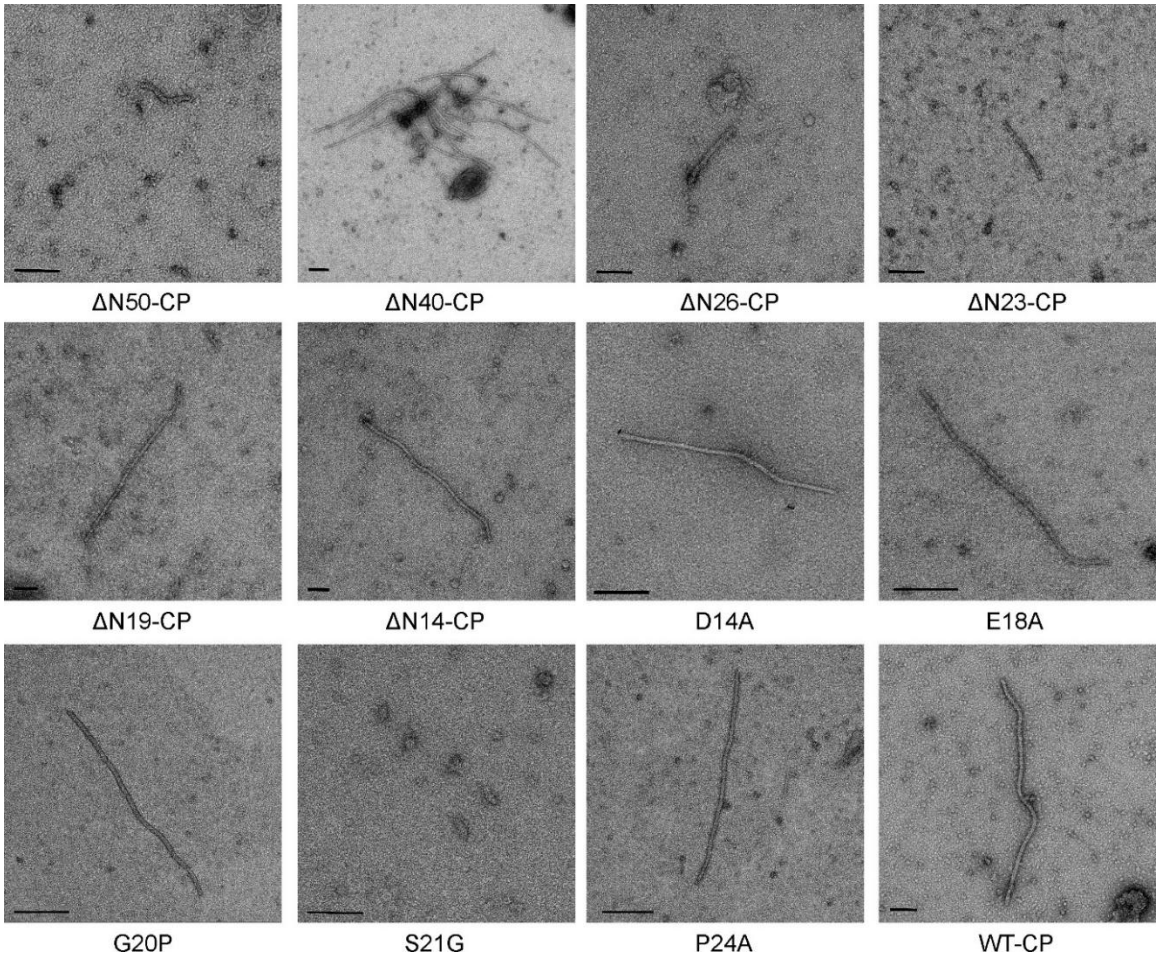

Fig. S10 Transmission electorn microscopy (TEM) micrographs of deletion and point mutants. Representative TEM micrographs of deletion mutants and point mutants. Results were obtained with negative staining. Scale bars for deletion mutants and WT-CP are 100 nm and for point mutations 200 nm except in case of S21G (50 nm). Additional images of the mutant viruses were deposited at Zenodo (doi: 10.5281/zenodo.17177382).

837
838 **Table S1. ΔN26-CP viral limitation on single cells or cell-to-cell spread.** Number of plants
839 with viral cell-to-cell spread or viral limitation to single cells 10 and 14 dpb. Note that 5 dpb virus
840 was limited to single cells in all observed plants.

		ΔN26-CP	**WT-CP**
10 dpb	single cells	3/8	0/2
	cell-to-cell	5/8	2/2

		ΔN26-CP	**WT-CP**
14 dpb	single cells	2/3	0/2
	cell-to-cell	1/3	2/2

841

842

843 **Table S2. Replication efficiency of ΔN40-CP and S21G mutant is the same as the one of**
844 **WT-CP PVY.** To confirm that detected fluorescent signal in ΔN40-CP and S21G PVY mutants,
845 was the consequence of viral replication and not the continuous expression of viral genes from
846 the original plasmid of PVY driven by the constitutive 35S promoter, ROI (regions of interests)
847 mean intensities of individual cells in confocal microscopy images were assessed. Mean
848 intensities in selected ROIs 5 dpb for ΔN40-CP (A) and S21G (B) compared to WT-CP PVY are
849 shown. Statistical significance of differences was evaluated using Welch`s t test. Note that all
850 images were taken using the same settings (objective, zoom, gain).

A)

ΔN40-CP	WT-CP	Welch`s t test
24.4	13.8	0.6
14.0	17.1	
9.7	15.5	
13.3	9.4	
8.4	15.2	
4.8	21.6	
11.5	13.7	
8.6	15.6	
13.1	8.7	
25.7	15.9	
13.3	**14.6**	**average**

B)

S21G	WT-CP	Welch`s t test
6.8	7.1	0.2
6.8	9.4	
6.8	12.8	
6.8	**9.8**	**average**

851

852

853